AAPS PharmSciTech (2020) 21:264
DOI: 10.1208/s12249-020-01805-x

Research Article

Preparation and Evaluation of Mebendazole Microemulsion for Intranasal Delivery: an Alternative Approach for Glioblastoma Treatment

Julio Mena-Hernández,[1,2] Helgi Jung-Cook,[2,3,8] Monserrat Llaguno-Munive,[4] Patricia García-López,[4] Adriana Ganem-Rondero,[5] Simón López-Ramírez,[6] Fernando Barragán-Aroche,[6] Marisol Rivera-Huerta,[7] and Lourdes Mayet-Cruz[2]

Received 1 June 2020; accepted 27 August 2020

Abstract. Although mebendazole (MBZ) has demonstrated antitumor activity in glioblastoma models, the drug has low aqueous solubility and therefore is poorly absorbed. Considering that other strategies are needed to improve its bioavailability, the current study was aimed to develop and evaluate novel microemulsions of MBZ (MBZ-NaH ME) for intranasal administration. MBZ raw materials were characterized by FTIR, DSC, and XDP. Subsequently, the raw material that contained mainly polymorph C was selected to prepare microemulsions. Two different oleic acid (OA) systems were selected. Formulation A was composed of OA and docosahexaenoic acid (3:1% w/w), while formulation B was composed of OA and Labrafil M2125 (1:1% w/w). Sodium hyaluronate (NaH) at 0.1% was selected as a mucoadhesive agent. MBZ MEs showed a particle size of 209 nm and 145 nm, respectively, and the pH was suitable for nasal formulations (4.5–6.5). Formulation B, which showed the best solubility and rheological behavior, was selected for intranasal evaluation. The nasal toxicity study revealed no damage in the epithelium. Furthermore, formulation B improved significantly the median survival time in the orthotopic C6 rat model compared to the control group. Moreover, NIRF signal intensity revealed a decrease in tumor growth in the treated group with MBZ-MaH ME, which was confirmed by histologic examinations. Results suggest that the intranasal administration of mebendazole-loaded microemulsion might be appropriated for glioblastoma treatment.

KEY WORDS: mebendazole; glioblastoma; intranasal administration; microemulsion; sodium hyaluronate.

[1] Programa de Maestría y Doctorado en Ciencias Químicas, Universidad Nacional Autónoma de México, 04510, México City, Mexico.
[2] Departamento de Farmacia, Facultad de Química, Universidad Nacional Autónoma de México, 04510, México City, Mexico.
[3] Laboratorio de Neuropsicofarmacología, Instituto Nacional de Neurología y Neurocirugía" Manuel Velasco Suárez", 14269, Mexico City, Mexico.
[4] Laboratorio de Farmacología, Subdirección de Investigación Básica, Instituto Nacional de Cancerología, 14080, Mexico City, Mexico.
[5] Laboratorio de Investigación y Posgrado en Tecnología Farmacéutica, Facultad de Estudios Superiores Cuautitlán, Universidad Nacional Autónoma de México, 54740, Edo de Mex, Mexico.
[6] Departamento de Ingeniería Química/USIP, Facultad de Química, Universidad Nacional Autónoma de México, 04510, Mexico City, Mexico.
[7] Unidad de Experimentación Animal, Facultad de Química, Universidad Nacional Autónoma de México, 04510, Mexico City, Mexico.
[8] To whom correspondence should be addressed. (e–mail: helgi@unam.com)

INTRODUCTION

Glioblastoma (GBM) is the brain tumor with the highest incidence, and its extremely aggressive nature contributes to very low patient survival (1). The gold standard treatment is radiotherapy and concomitant chemotherapy with temozolomide, rendering an average survival time of 14.6 months (2). The challenges of GBM chemotherapy include its low efficacy, the limited number of therapeutic alternatives, the restricted access of molecules to the brain, and the elevated cost of available drugs (3). Thus, new therapeutic options are urgently needed for this cancer.

Mebendazole (MBZ), an anthelmintic drug used in patients with parasitic infections for over 30 years, has shown significant antiproliferative activity in glioblastoma models (4,5). The known safety profile and high potency have positioned it as an attractive candidate for GBM management. However, the drug exhibits extremely low aqueous solubility, which causes poor and erratic absorption from the gastrointestinal tract, and therefore, its bioavailability is low (5 to 10%) (6). Moreover, it exhibits a high hepatic

Published online: 27 September 2020

metabolism. Therefore, it is necessary to develop new and safe strategies for the use of mebendazole for this treatment.

Recently, there is a growing interest in intranasal administration as a drug delivery method due to its capacity to transport the drug directly to the brain along the olfactory and trigeminal nerves (7,8). Subsequently, the drug is transported into the cerebrospinal fluid or brain tissue (9). Since the blood-brain barrier (BBB) is circumvented, the doses employed by this route could be lower than by oral administration. Additionally, the extensive vascularization of the large nasal surface area, allows the drug to avoid hepatic metabolism (9). Hence, this route has been proposed as a potential alternative for the delivery of antineoplastic drugs in the treatment of GBM (10–12).

Microemulsions (MEs), which are versatile lipid-based drug delivery systems, offer several advantages such as the capability to enhance the solubility of many lipophilic drugs, a spontaneous formation, easiness to manufacture, and scale-up. They are clear, stable, isotropic mixtures of oil, water, and surfactant, frequently in combination with a cosurfactant. (13).

Increasing evidence suggests that the intranasal administration of drugs in microemulsions is safe and effective. In this context, an increase in brain concentrations of saquinavir mesylate (14), albendazole sulfoxide (15), and teriflunomide (16) concentrations were recently reported. The aim of the current study was to formulate and characterize microemulsions with sodium hyaluronate (NaH) as a mucoadhesive agent for the intranasal administration of MBZ and to evaluate the efficacy of the best formulation in an orthotopic rat model of glioblastoma.

MATERIALS AND METHODS

Materials

Three batches of MBZ, two from KA Malle Pharmaceutica Ltd. (Gujarat, India) and one analytical standard from Sigma-Aldrich (Steinheim, Germany), were characterized. Transcutol HP, Labrafac, Labrafil M 2125, Labrasol, and Peceol were kindly provided by Gattefossé, (Saint-Priest Cedex, France). Super refined oleic acid (OA) and docosahexaenoic acid-rich oil (enriched fish oil, DHA 500 TG-LQ-LK) were generously provided by Croda Inc. (East Yorkshire, UK). Tween 80 was purchased from Sigma-Aldrich (Steinheim, Germany). Sodium hyaluronate (NaH, MW 1900 kDa) was donated by DSM Nutritional Products Ltd. (Kaiseraugst, Switzerland). Distilled or deionized water was obtained from the Elix 3 and Milli-Q water purification system (Millipore, Milford, MA, USA). The solvents employed in the chromatographic analysis were HPLC grade (JT Baker). All other reagents and solvents were of analytical grade.

METHODS

Characterization of Mebendazole Raw Material

The three batches of MBZ were characterized by means of Fourier-transform infrared spectroscopy (FTIR), X-ray powder diffraction (XRPD), and differential scanning calorimetry (DSC). The infrared spectra were obtained using on a Perkin-Elmer Model Spectrum 400 spectrophotometer. Data were collected over a spectra region from 4000 to 400 cm^{-1} with a resolution of 4 cm^{-1}. X-ray diffraction patterns were acquired on a Siemens D-5000 D8 Advance diffractometer with a Cu monochromator. Samples were examined in the 2θ angle range of 3–40° and an acquisition time of 28 min. DSC measurements were obtained using calorimeter Mettler-Toledo Star system. Samples of 2–4 mg were weighed, placed in aluminum pans, sealed, and heated at a rate of 10°C/min in the temperature range of 80 to 320°C with a 100 mL/min flow of air.

Solubility Study

In order to select the oily phases, surfactants and cosurfactants for the preparation of microemulsions, the solubility of MBZ was determined in the following excipients: OA, soybean oil, docosahexaenoic acid (DHA), isopropyl myristate, Peceol, Labrafac, Labrasol, Labrafil M 2125, Tween 80, Transcutol HP, Cremophor RH 40, polyethylene glycol 400 (PEG), propylene glycol, and ethanol. Briefly, an excess of the drug was added to each glass tube containing 2 mL of the corresponding vehicle, and the mixtures were maintained in a shaker water bath for 48 h at 25°C. Then, each sample was centrifuged at 4000 rpm for 15 min. The supernatant was properly diluted with methanol, and the MBZ concentration was determined by HPLC (Shimadzu LC-10ATvp) using an Eclipse® XDB-C8 column (4.6 × 150 mm) particle size 5 μm (Agilent). The mobile phase was methanol:water (60:40) at a flow rate of 1.2 mL/min and a UV detector at 247 nm. The analysis was carried out at 25°C. The method was linear in the range of 1.5–51.0 μg/mL. Intra-day and inter-day coefficients of variation were < 2%.

Pseudo-Ternary Phase Diagrams

Based on the solubility results, OA and its combination with DHA and Labrafil M 2125 were chosen as the oil phase (O) in ratios of 3:1 and 1:1 w/w, respectively. Tween 80, Transcutol HP, and ethanol were selected as the surfactant, cosurfactant and cosolvent, respectively, and were used in different proportions (1:1:1, 2:1:1, 3:1:1, 1:2:1, 1:1:2, 1:1:3% w/w) to elaborate various mixture systems (Smix). Each ratio of Smix was mixed with the oil phase under magnetic stirring until a homogeneous appearance was achieved. Subsequently, distilled water was added in a dropwise manner, recording the volume at which the system changed from transparent to opaque. Based on the proportions calculated for each component, pseudo-ternary phase diagrams were constructed using OriginLab software (Northampton, MA, USA). All samples exhibiting a transparent and homogeneous state were assigned to a microemulsion region in the phase diagram.

Preparation of MBZ-Loaded MEs

According to the microemulsion formation zones defined in the pseudo-ternary phase diagrams, two different formulations were selected. Formulation A was composed of 9% OA/DHA at a ratio of 3:1 (w/w), 51% Smix and 40% water, while

formulation B consisted of 10% OA/Labrafil M 2125 in a ratio of 1:1 (w/w), 51% Smix and 39% water.

Formulation A was elaborated by solubilizing MBZ in Transcutol HP and subsequently adding OA and DHA under gentle magnetic stirring, followed by Tween 80 and ethanol. Finally, water was slowly added. For formulation B, MBZ was solubilized in Labrafil M 2125 at 50°C in a water bath under constant magnetic stirring. Later OA was added and the temperature was allowed to decrease to room temperature. Transcutol HP, Tween 80, and ethanol were added under magnetic stirring before slowly adding water. In the case of the microemulsion containing NaH (MBZ-NaH ME), the biopolymer (0.1% w/w) was solubilized in the aqueous phase, then slowly integrated into the lipid-Smix mixture. The drug content was determined by HPLC at 247 nm after diluting the microemulsions with methanol.

Physicochemical Characterization of MBZ-Loaded Microemulsions

The particle size, polydispersity, and zeta potential of the microemulsions were determined by the dynamic light scattering technique at 25°C on a Malvern Zetasizer Nano ZS-90 apparatus (Worcestershire, UK). The pH values were measured at 25°C on a pH Orion Star Benchtop Meter (Thermo Scientific, MA, USA), while conductivity was assessed with a Hanna Instruments waterproof tester (Woonsocket, RI, USA). Morphology was examined by transmission electron microscopy (TEM). The microemulsions were placed onto a film-coated copper grid prior to negatively staining the samples with 2% p/v of phosphotungstic acid (Agar Scientific, Essex, UK) and allowed to dry at room temperature. Samples were observed using a TEM Jeol 2010 apparatus (MI, USA) and 200 kV of accelerating voltage. The physical stability of the formulations was determined by centrifugation (4000*g* for 15 min) and thermal stress (50°C for 48 h). Changes such as phase separation, flocculation, or creaming were evaluated. The MBZ content was monitored for 89 days at room temperature using the previously described HPLC assay.

Rheological Study

A controlled stress Discovery Hybrid Rheometer (DHR3) from TA Instruments (Delaware, USA) with a double wall cylinder concentric geometry was used for rheological and viscoelastic analysis through rotational and oscillatory tests at 25°C, respectively. A sweep from 0.01 to 100 s^{-1} was achieved to analyze the shear rate ($\dot{\gamma}$) dependence of viscosity (μ). The storage (G′) and loss (G″) moduli were measured using the controlled strain and angular frequency options. Since G′ and G″ were independent of the strain amplitude over the linear viscoelastic region, the latter was determined with a strain sweep from 0.01 to 100% at a fixed angular frequency of 10 rad s^{-1} (1.5915 Hz). Considering the experimental results, both G′ and G″ were independent of the applied strain below of 10%, that is, a linear viscoelastic behavior was observed below this deformation, therefore, the viscoelastic behavior of the formulations was examined by applying a constant deformation of 1% over a frequency range between 0.1 and 10 Hz. Finally, a sweep from 20 to 40°C at a constant shear rate of 1 s^{-1} was performed to check the temperature dependence of viscosity and thus discard the possibility of emulsion phase inversion.

Nasal Toxicity Test

Male Sprague-Dawley rats (200–250 g), acquired from Envigo CRS Limited, were acclimated for 5 days under standard housing conditions with a 12-h light/dark cycle, a temperature of 21 ± 2°C, and humidity at 40–70%. Food and water were provided *ad libitum*. The protocol was approved by the Institutional Committee for Animal Handling and Care of the Facultad de Química at the Universidad Nacional Autónoma de México (number FQ/CICUAL/348/18) and was carried out according to Mexican Regulations for Animal Experimentation (NOM-062-ZOO-1999).

Eighteen rats were assigned randomly to the following groups: group I, saline solution (negative control); group II, the vehicle of formulation B (NaH ME), and group III, formulation B (MBZ-NaH ME). Twenty microliters of the treatments were applied in each nostril for 14 days. Animals were weighed on days 0, 7, and 14. Behavior and clinical observations were made every day throughout the study.

Immediately after, the rats were sacrificed with carbon dioxide gas and decapitated. The nasal tissue was extracted and evaluated macroscopically. The samples were fixed in 10% formalin and divided into three sections: cranial nasal epithelium (near the nostril), the middle nasal epithelium (middle part of the nasal cavity), and caudal nasal epithelium (ethmoidal shells). The tissues were dehydrated, embedded in paraffin, sliced into 3 μm thick sections, stained with hematoxylin and eosin, and analyzed by light microscopy.

In Vivo Efficacy Study of MBZ-NaH ME in an Orthotopic Model of Glioblastoma

Animals and Cell Culture

Male Wistar rats (200–230 g) were supplied by Universidad Autónoma Metropolitana (UAM), Mexico City, Mexico. All procedures for the care and handling of the animals were approved by the Ethics Committee of the Instituto Nacional de Cancerología of Mexico (numbers 010/017/IBI and CEI/601/109) and were in accordance with the Mexican Regulations for Animal Experimentation and Care (NOM-062-ZOO-1999).

The C6 rat glioma cell line, obtained from American Type Culture Collection (Rockville, MD, USA), was routinely maintained as a monolayer in DMEM supplemented with 5% fetal bovine serum. The cells were incubated at 37°C in a 5% CO_2 atmosphere at high humidity and harvested with 1 mM EDTA.

Tumor Cell Implantation

The efficacy of the orthotopic C6 rat glioma model was determined by the method of Llaguno et al. (17). Briefly, each animal was placed in a stereotactic device for surgery following anaesthetization with a combination of tiletamine hydrochloride (10 mg/kg) and acepromazine maleate (0.4 mg/kg) i.m. After fastening the head in the frame, a

midline incision was made and bregma was identified. The skull was then drilled at the coordinates of 2.0 mm right from bregma and 6 mm deep, in accordance with the Paxinos and Watson atlas (18). C6 cells were harvested, washed two times, and diluted in DMEM to a concentration of 1.0×10^6 in a volume of 3 μL. Through a 27-gauge needle connected to an infusion pump, these cells were slowly implanted at a depth of 6 mm from the dura mater. The scalp was closed and the rat was returned to the animal facility. The sham group underwent the surgical procedure only, without the implantation of tumor cells. Animals were subsequently weighed throughout the experiment.

Intranasal Administration of Treatments

One week after implantation of tumor cells, the rats were divided into four groups ($n = 6$): the sham-operated animals (without glioma cell inoculation and in the absence of treatment) and three groups that received a glioma cell implantation, including the control (without treatment), the group given NaH ME (the vehicle of formulation B) and the one receiving MBZ-NaH ME (an MBZ-loaded microemulsion containing formulation B at 260 μg/mL). The intranasal administration was based on reports by Stenslik et al. (19). The rats were anesthetized in an induction chamber with isoflurane at 1.0–3.0% and 100.0% oxygen before 40 μL of the treatments were applied by using a plastic tip, which was placed 3 mm inside the animal nose with the head upward. This procedure was carried out every day for 14 days.

Evaluation of Tumor Growth

Tumor growth was evaluated by monitoring animal weight loss and survival time throughout the 50-day experiment. At the end of each treatment, the effect on tumor growth was assessed with the contrast agent (IRDye® 800CW RGD Optical Probe; abs: 776 nm; em: 792 nm; LI-COR Biosciences) which is a near-infrared fluorescence (NIRF) imaging agent specifically designed to target integrins. Briefly, 1 nmol of IRDye 800CW RGD was injected into the caudal vein of the rats under O_2/isoflurane anesthesia (1–3% isoflurane in 100% oxygen). At 48 h post-injection, the animals were euthanized to prepare for dissection of the brain. Optical imaging was captured with the Odyssey Infrared Imaging System (LI-COR), and the absolute fluorescence intensities were quantified on Odyssey Application Software. The regions of interest and background were selected. Background fluorescence was subtracted from the signal intensities, and the fluorescence signal/area was the basis of comparison between groups.

Histological Analysis

At the end of the experiment, all rats were euthanized and perfused, first using a saline solution and then 4% paraformaldehyde. The brain tissue was embedded in paraffin to be sliced into 2-mm-thick sections on the coronal plane. The tissue slices were stained using the hematoxylin-eosin method.

Statistical Analysis

Differences between groups were examined with one-way analysis of variance (ANOVA) on GraphPad Prism software (San Diego, CA, USA), followed by the Bonferroni multiple comparisons test. In all cases, significance was considered at $p < 0.05$.

RESULTS AND DISCUSSION

Characterization of MBZ Raw Material

The raw material of MBZ is comprised of a mixture of three polymorphic forms, designated as A, B, and C. Polymorph B is the most soluble form and polymorph A the most insoluble (20). Each form exhibits distinct antitumor activity (21). Pure polymorph C has been recommended for its use as an anticancer agent due to its solubility and thermodynamic stability (22). However, the cost of producing polymorph C is high, and there is evidence of the transition from polymorph C to polymorph A during the manufacturing and packaging process (23). Therefore, it was considered important to develop the formulations using mebendazole raw material.

In the present study, the three batches of MBZ were characterized in order to determine whether they contained polymorph C. The IR spectra of the three batches showed a 3410 cm^{-1} signal, attributed to the –NH bond of polymorph C, (Fig. 1a). In MBZ-02, the characteristic signals at 3370 cm^{-1} for the –NH bond of polymorph A and 3340 cm^{-1} for polymorph B were not found (24). Concerning the XRPD analysis, Brits et al. (25) described the following inter-planar distances for the three MBZ polymorphs: 7.67 d (Å) for polymorph A, 5.84 d (Å) for polymorph B and 4.93 d (Å) for polymorph C. The peak for polymorph C was detected in the diffractograms of MBZ-01, MBZ-02, and MBZ-03 (Fig. 1b), but the peak for polymorph B did not appear in MBZ-02 batch. The DSC thermograms of the samples showed two endothermic events (Fig. 1c). The first endothermic transition peak was detected at 231°C, 240°C, and 223°C for MBZ-01, MBZ-02, and MBZ-03, respectively. The second endothermic peak around 310°C was found in all three polymorphs (26). MBZ-02 also displayed an exothermic peak at 185°C, which could be attributed to the transition from polymorph C to the A form by a crystal arrangement (20).

Solubility Study

Oils and surfactants were chosen for evaluation in the current investigation based on the safety profile documented by previous studies of nasal administration (15,27–32). The solubility of MBZ was examined in the different oils, surfactants, cosurfactants, and cosolvents (Fig. 2). The solubility of MBZ in soybean oil, Peceol, Labrafac, and Labrasol was in the range of 112–326 μg/mL. The greatest solubility was found in OA (1305 ± 59 μg/mL). Although the solubility of the drug was not increased by the combination of OA with DHA at a 3:1 ratio (1231 ± 27 μg/mL), it has been reported that DHA in microemulsions can improve the nose to brain delivery of drugs (15,33). OA/Labrafil at a 1:1 ratio

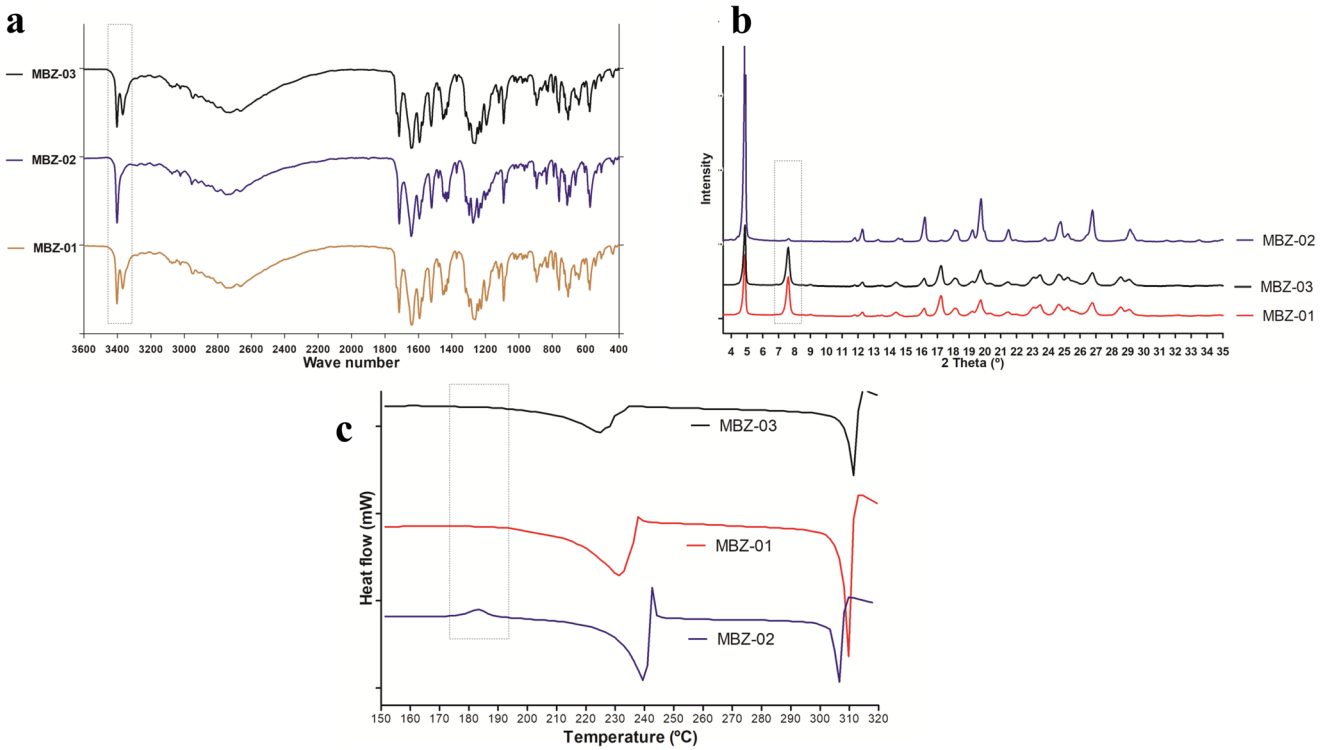

Fig. 1. **a** FT-IR transmittance spectrum, **b** X-ray powder diffractogram, and **c** DSC thermograms of three mebendazole raw materials evaluated

(1737 ± 68 μg/mL) also considerably enhanced MBZ solubility. Thus, for the construction of the pseudo-ternary phase diagrams, mixtures of OA/DHA and OA/Labrafil M 2125 were selected. Labrasol, Tween 80, Transcutol, and PEG were employed as nonionic surfactants because of the good MBZ solubility results with these compounds (1660 ± 09 μg/mL, 1129 ± 14 μg/mL, 2019 ± 17 μg/mL, and 1349 ± 25 μg/mL, respectively).

Pseudo-Ternary Phase Diagrams

The pseudo-ternary phase diagrams for the microemulsions of both oily phases (OA/DHA and OA/Labrafil M 2125) using the Tween 80/Transcutol HP/ethanol mixture (Smix) at two distinct ratios (1:1:1 and 1:2:1) revealed a limited capability to incorporate water (Fig. 3). There was a larger microemulsion region in the OA/Labrafil M 2125 (Fig. 3b) than OA/DHA mixture (Fig. 3a). This may be related to the composition of Labrafil M 2125, being a mixture of medium and long-chain fatty acids. Consequently, the penetration of OA into the surfactant monolayer was restricted. Labrasol and PEG were discarded due to their reduced microemulsion formation area.

Preparation of MBZ-Loaded MEs

The use of the spontaneous emulsification method (titration method) at room temperature was appropriate to prepare mebendazole-loaded microemulsions. Formulation B required a heating stage (at the temperature recommended by the manufacturer) for Labrafil M 2125 homogenization. The drug content assay showed that almost twice of the drug load was achieved with formulation B (260 ± 3.36 μg/mL) *versus* formulation A (154 ± 1.7 μg/mL).

It has been shown that nasal microemulsions with mucoadhesive molecules prolong the retention time and thus, improve the absorption of drugs in the CNS (27). Sodium Hyaluronate (NaH) at 0.1% was added to both formulations (MBZ-NaH MEs) due to its biodegradability, biocompatibility, and good mucoadhesive properties (34). No changes in appearance, color, or precipitation were observed.

Physicochemical Characterization of Mebendazole-Loaded Microemulsions

Table I shows the physicochemical properties for drug-free and drug-loaded formulations. As can be appreciated, the incorporation of the drug did not substantially modify the properties of the microemulsion in either of the two systems. The particle size distribution (PSD < 210 nm) is viable for nasal administration. Polydispersity values were under 0.7, suggesting an acceptable distribution (35). Despite the low value of the zeta potential (less than − 0.3), the microemulsions maintained their appearance after undergoing mechanical and thermal stress. The pH was in the range of 4.5–6.5, considered acceptable for nasal administration (36). The conductivity values (17–30 μS/cm) indicate an oil-in-water type system, which is favorable for nasal administration. Transmission electron microscopy (TEM) analysis revealed a spherical morphology for both formulations (Fig. 4). The drug content > 93% of formulation B (MBZ-NaH ME) was maintained following 89 days of storage at room temperature (25°C).

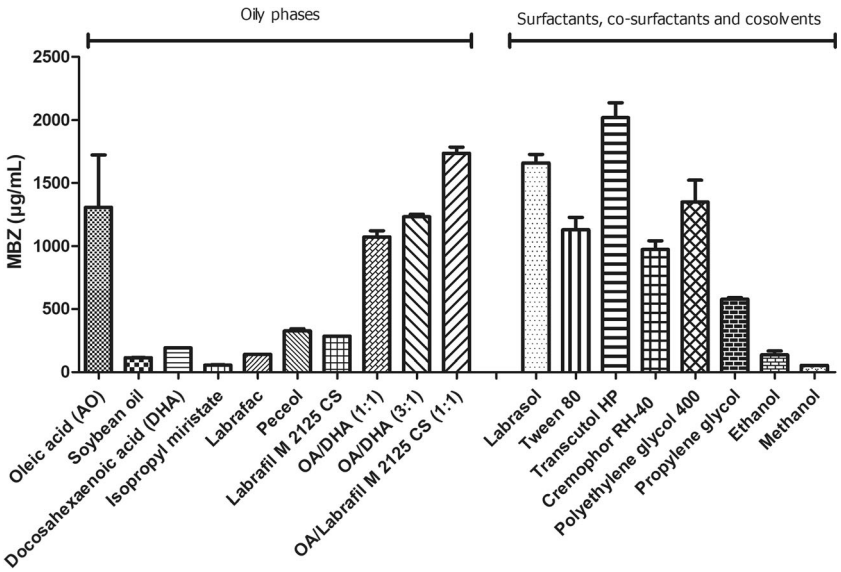

Fig. 2. Solubility of mebendazole in different oils, surfactants, cosurfactants, cosolvents, and mixtures. Data are expressed as the mean ± SD ($n = 3$)

Rheological Study

Flow curves were used to understand the interaction of the components in the formulations. The MEs showed a linear relationship between shear rate and shear stress, indicating a Newtonian behavior (Fig. 5). No changes in viscosity were observed in either formulation (ME) after the encapsulation of MBZ (MBZ ME) (Fig. 5a and b), which indicates that the components of the microemulsion in both formulations (A or B) did not interact with MBZ. The incorporation of NaH in the microemulsion without MBZ (NaH ME) increased the viscosity and promoted a non-Newtonian behavior, an indicator of a pseudoplastic fluid. A higher viscosity was found when MBZ was incorporated in formulation A, MBZ-NaH ME (Fig.5a), suggesting intermolecular interactions such as hydrogen bonds between the –NH or –OH of NaH and –HC=CH–, –H of DHA or = N–H of the tautomeric form of MBZ. In formulation B (Fig. 5b), no difference in viscosity was detected between NaH ME and MBZ-NaH ME. Hence, formulation B was chosen for the further evaluations.

Viscoelasticity

According to the viscoelastic behavior of ME, MBZ ME, NaH ME, and the formulation B (MBZ-NaH ME), the values of G′ (Fig. 5a) and G″ (Fig. 5b) increased in the entire frequency range. The presence of NaH had more impact on the increment of both moduli. These results could be explained by the hydrogen bond formation between the water molecules and the carboxylic groups of the hyaluronate sodium molecules, generating a dynamic network and hence an increment of rigidity of sample. The loss factor (tan δ) corresponds to the ratio of the loss modulus to storage modulus. An increase in this parameter gives rise to the predominance of viscous behavior in the system. Although all

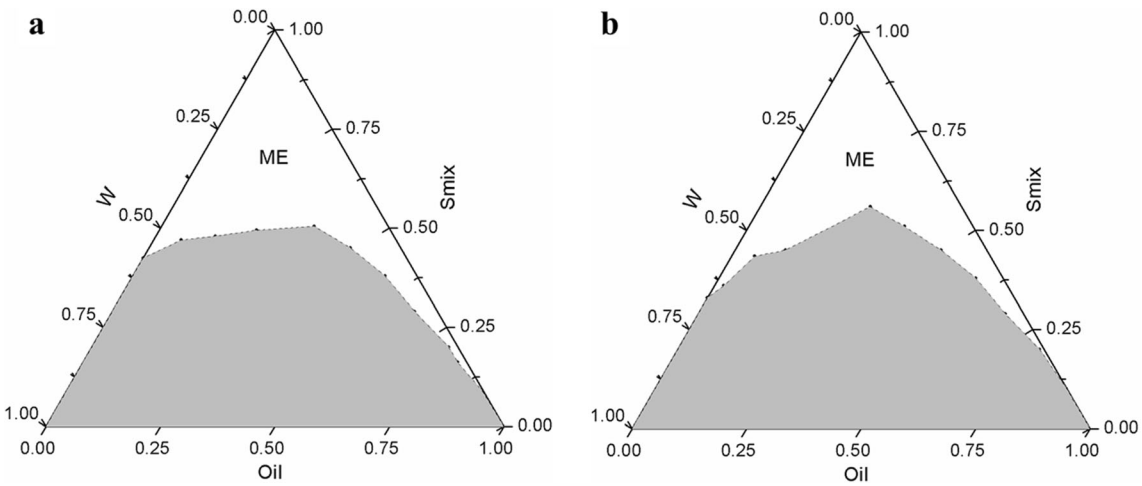

Fig. 3. Pseudo-ternary phase diagrams for the oily phases: **a** oleic acid/DHA (3:1 w/w) with a Smix of Tween 80/Transcutol HP/ethanol (1:1:1 w/w) and water (W), and **b** oleic acid/Labrafil M 2125 (1:1 w/w) with a Smix of Tween 80/Transcutol HP/ethanol (1:2:1 w/w) and water (W)

Table I. Physicochemical characterization of the drug-free and mebendazole-loaded microemulsions in both formulations

Microemulsion systems	MBZ (μg/mL)	Particle size (nm)	Zeta potential (mV)	Polydispersity index	pH	Conductivity (μS)
Formulation A	———	115.7	− 0.378	0.576	5.03	27
	130	209	− 0.056	0.439	5.08	31
Formulation B	———	129.6	− 0.203	0.432	5.38	17
	250	145	− 0.119	0.444	5.36	20

samples had a predominant viscous behavior (Fig. 6c), a greater elastic behavior was displayed by the formulations with NaH. The increase of G′ behavior plays a rule of paramount importance, as the hypothesis states that, when nasal microemulsions are deposited as a thin layer on the nasal mucosa, the carboxylic group of NaH interacts with calcium ions present in the mucosa fluid. If there is a sufficient concentration of these ions, a gel is formed. In the gel state, if the residence time of the formulation on the mucosal surface is prolonged and the drug will be released in a controlled manner (37). Formulation B showed a temperature-dependent viscosity without any emulsion phase inversion in the range of temperatures evaluated (Fig. 6d).

Nasal Toxicity Test

Although MBZ pharmacology, safety, general toxicity, and carcinogenicity are extensively known (4), the specific nasal toxicity has not been evaluated. Results showed that exposure to MBZ-NaH ME over 14 days did not cause any loss of hair, hemorrhages, diarrhea, or behavioral modifications. The macroscopic evaluation from the nasal vestibule to nasopharynx did not reveal changes in the color, redness, or texture of the tissue compared to the control group. Figure 7 shows the histopathological images of the nasal cavity regions following the application of the saline solution and MBZ-NaH ME. No changes were found (*e.g.*, necrosis, cell degeneration, or leucocytic infiltration) in cranial, middle, or caudal sections. Although the epithelium tissue was diminished, the nasal membrane maintained its integrity with the application of formulation B, and no histopathological alterations were observed in the regions evaluated, nor were there any significant differences in the body weight between the MBZ-NaH ME and the control group (Fig. 7g). These results suggest that the nasal administration of the formulation at the dose tested is safe and appropriate.

In Vivo Efficacy of MBZ-NaH ME in an Orthotopic Model of Glioblastoma

Since glioblastoma is the most aggressive primary brain tumor, the patient survival rate is low. The antitumor activity of MBZ demonstrated *in vitro* and *in vivo* represents an attractive alternative for therapy. However, its oral administration has shown a low absorption. Thus, the antitumor activity of intranasally administered MBZ-NaH ME was examined on an orthotopic model of glioma cells implanted intracranially in rats, which is widely used to analyze the efficacy of a variety of treatments (38). The model exhibits several characteristics observed in human glioblastoma, such as high mitotic index, focal tumor necrosis, parenchymal invasion, neovascularization, and global transcriptomic profiles (39,40).

Additionally, tumor growth can be indirectly assessed by means of animal weight loss. Results showed that subsequent to glioma cell implantation, all animals gained weight during the first few days and underwent a drastic weight loss as of day 9 (Fig. 8a). The latter reduction in body weight is attributed to tumor growth. The sham group did not show any weight loss, verifying that the surgical interventions did not contribute to a toxic effect. On the other hand, the rapid weight loss of the control group strongly suggests accelerated tumor growth. There was significantly less weight loss in the MBZ-NaH ME rats compared to those receiving the vehicle (NaH ME) or no treatment (the control).

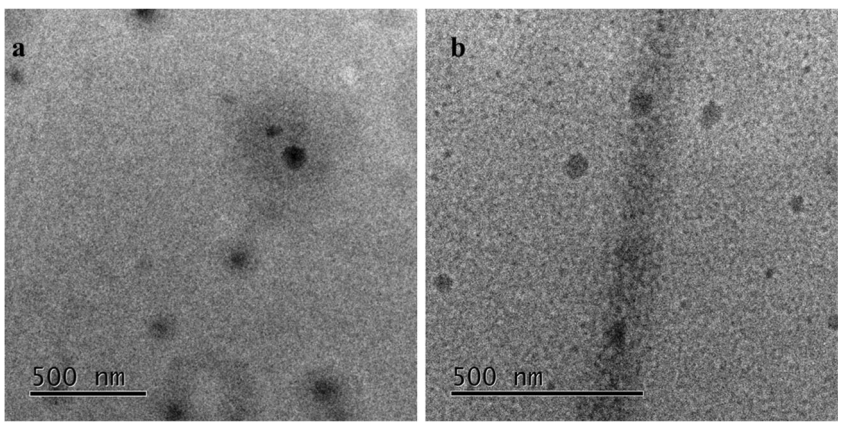

Fig. 4. TEM images of the microemulsions with mebendazole and sodium hyaluronate: **a** formulation A and **b** formulation B

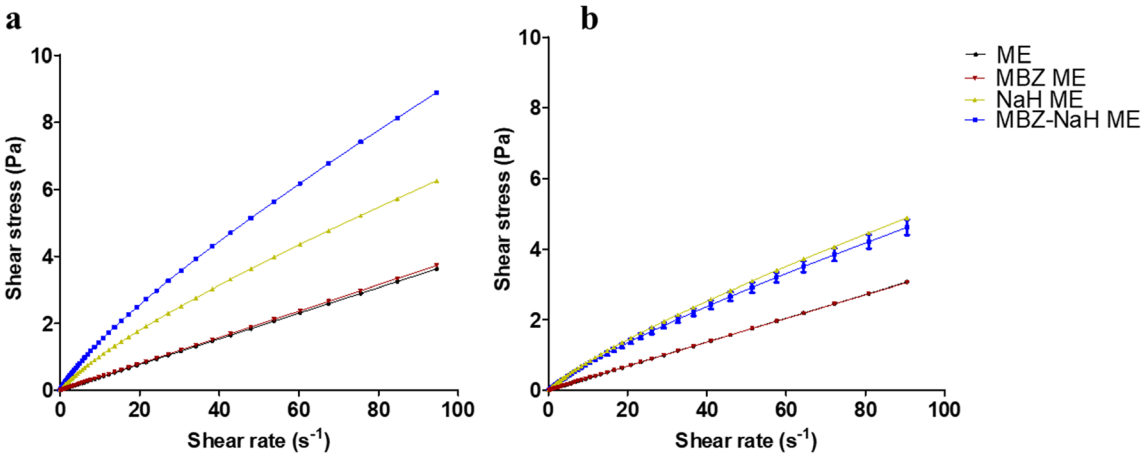

Fig. 5. Flow curves of **a** formulation A and **b** formulation B. ME microemulsion alone, MBZ ME microemulsion with mebendazole, NaH ME microemulsion with sodium hyaluronate, MBZ-NaH ME microemulsion with mebendazole and sodium hyaluronate ($n = 3$)

Animal survival time is another indicator of tumor growth. Whereas the animals in the control and NaH ME groups survived 20–30 days, those receiving MBZ-NaH ME were still alive at the end of the experiment (at day 50) (Fig. 8b). This effect could be attributed to the presence of OA in the microemulsion since an *in vitro* study demonstrated that oleic acid had an inhibitor effect in fatty acid and cholesterol synthesis on the C6 cell line (41). The current findings provide evidence of the capacity of MBZ-loaded microemulsion to arrive at the brain when delivered in the nasal cavity.

Theoretically, the biopharmaceutical properties of MBZ, especially its lipophilic behavior and small size, could favor its passage through nasal cells of the olfactory epithelium. Previously, in a clinical study, it was confirmed that MBZ crosses the BBB when given orally, but the concentrations are lower than in serum (42). Recently, it was reported that MBZ crosses the BBB with a brain/plasma (B/P) ratio of 0.80 for polymorph C and 0.64 for polymorph B (21). According to the present data, the nasal administration of 40 μL of MBZ-NaH ME at 250 μg/mL led to a survival rate similar to that described by Bai *et al.* (21) following oral administration of 50 mg/kg/day of polymorph C.

NIRF *Ex Vivo* Imaging Study

Fluorescence imaging has been instrumental for examining the efficacy of treatments and diagnosing tumors. It was herein employed as a third indicator of tumor growth. The fluorescent dye targets integrins, which are cell surface glycoproteins. Integrin α5β3 is highly expressed in glioma tumors, being involved in tumor growth, tumor invasiveness,

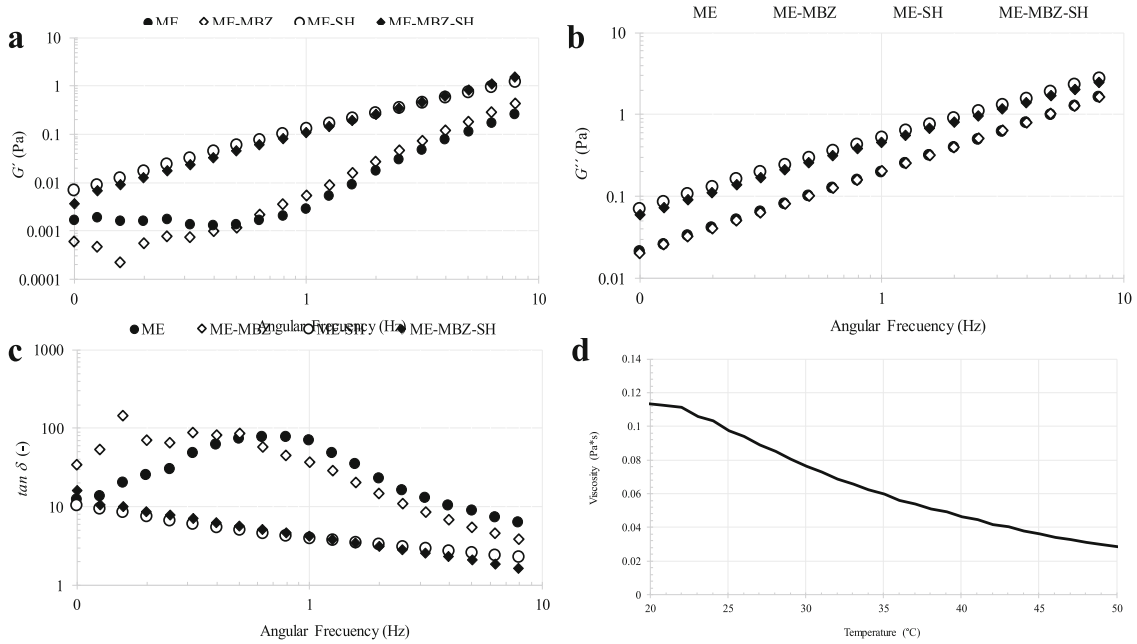

Fig. 6. Angular frequency dependence of the viscoelasticity behavior of formulation B: **a** elastic modulus (G′), **b** viscous modulus (G′′), **c** loss factor (tan δ), and **d** temperature dependence of viscosity. ME (solid circles), MBZ ME (blank diamonds), NaH ME (blank circles), and MBZ-NaH ME (solid diamonds)

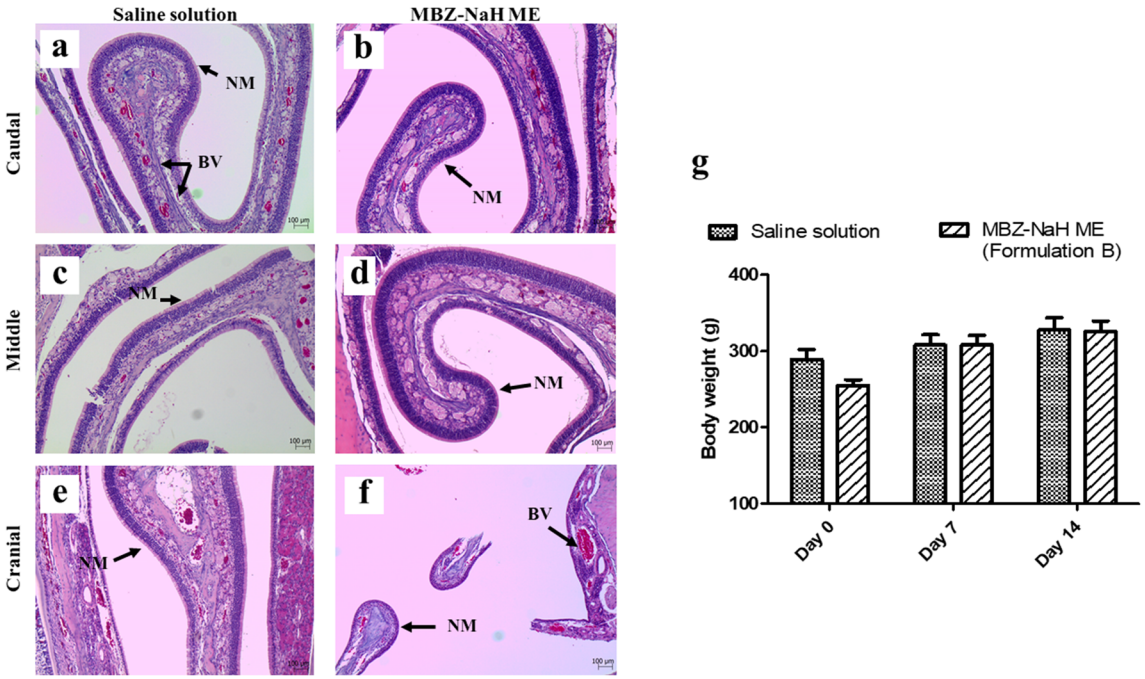

Fig. 7. Photomicrographs of the epithelium of three nasal regions after exposure to saline solution or formulation B (MBZ-NaH ME): caudal (**a**, **b**), middle (**c**, **d**), and cranial (**e**, **f**). NM nasal membrane, BV blood vessels. The body weight of rats during the nasal toxicity test is also presented (**g**). Data are expressed as the mean ± SD ($n = 6$)

metastasis, and angiogenesis. Arg-Gly-Asp (RGD) is a tripeptide sequence that binds to integrin receptors such as αvβ3. There are several reports of fluorescent labeling with RGD used for *in vivo* imaging (43). Regarding glioblastomas, the IRDye 800CW RGD probe targets the overexpressed integrin receptors, and then the tumor can be visualized with imaging. After the development of near-infrared fluorophores (NIRF) improved optical imaging, this technique was applied to an orthotopic glioblastoma model (44). Thus, a NIRF *ex vivo* imaging study was carried out to examine tumor size in the distinct groups of the current study (Fig. 9). As can be appreciated, fluorescence intensity was undetectable in the sham group and the glioma cell implantation groups on day 0, but was indeed detectable in the latter groups on day 7. Thus, the presence of a tumor was corroborated on the day the treatments began. The fluorescence signal was less intense in the NaH ME *versus* the control group, although the greatest reduction in signal intensity was observed with the MBZ-NaH ME treatment (Fig. 9a). Semiquantitative analysis was performed to determine the relative fluorescence intensity of IRDye 800CW RGD signals in the three groups with tumors. Results showed significant differences between the animals receiving MBZ-NaH ME and the control or NaH ME group (Fig. 9b). Hence, the MBZ formulation seems to have inhibited tumor growth. However, further research is needed in order to determine the molecular mechanisms of MBZ that support our findings.

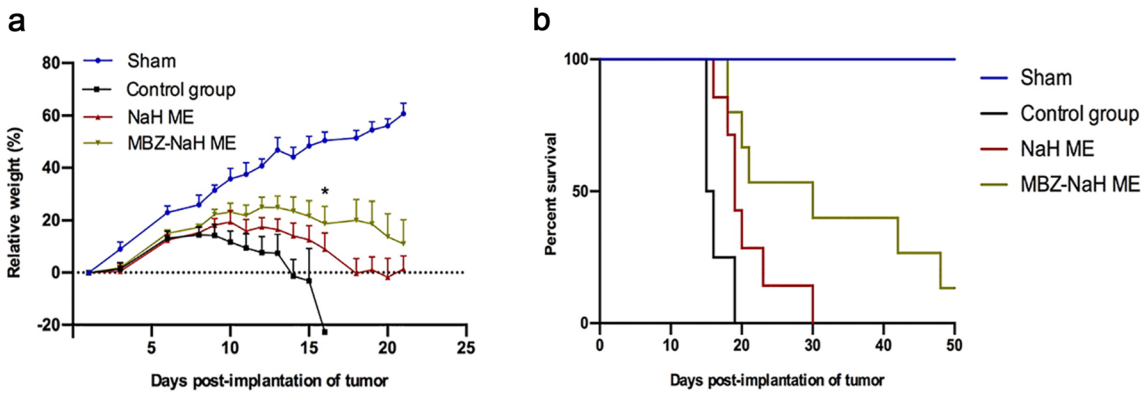

Fig. 8. Efficacy of the intranasal administration of a mebendazole-loaded microemulsion to inhibit tumor proliferation in an orthotopic rat model of glioblastoma, evaluated by weight loss and overall survival. **a** The relative weight of the animals was tracked for the distinct groups, including sham surgery (without tumor cell implantation and in the absence of treatment) and three groups that underwent the implantation of tumor cells, including the control (no treatment), NaH ME (vehicle), and MBZ-NaH ME (mebendazole-loaded microemulsion). **b** The survival of each group was monitored for up to 50 days post-implantation. *Significant difference ($p < 0.05$). Each point depicts the mean ± SEM of six animals

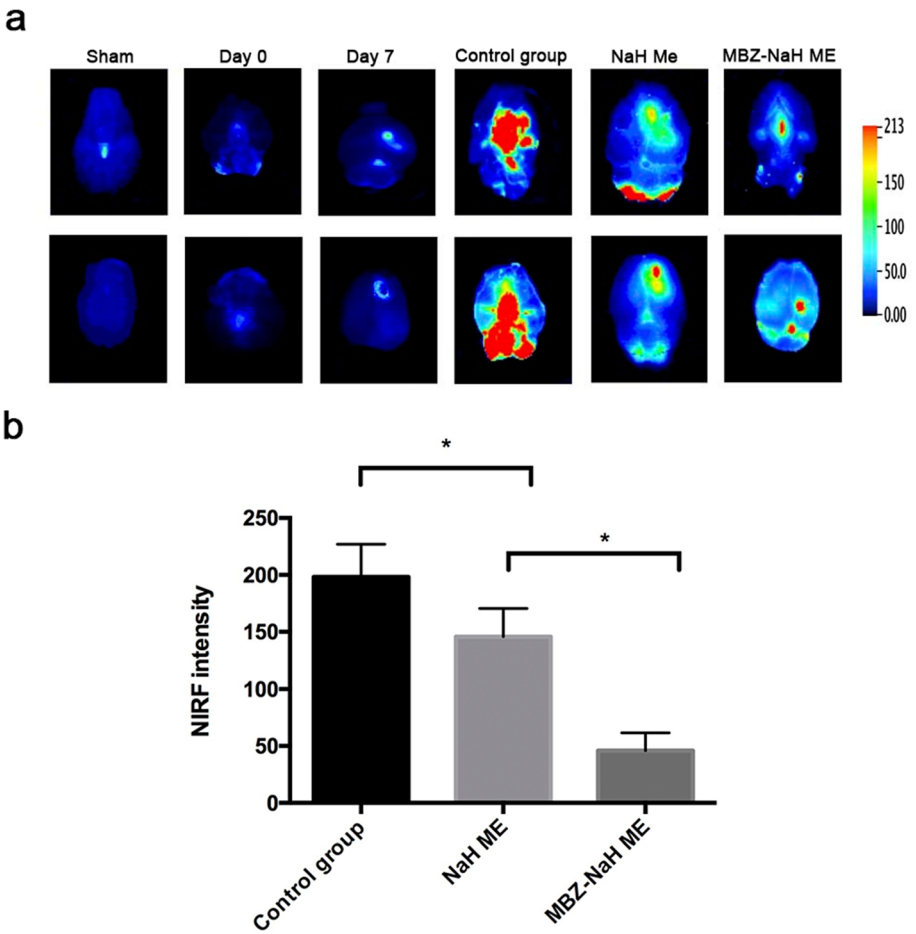

Fig. 9. **a** NIRF images show tumor uptake of IRDye 800CW RGD in the distinct groups and at two different times: sham (without glioma cells or treatment), on day 0 of glioma cell implantation, on day 7 post-implantation, the control (with implantation of glioma cells and in the absence of treatment), the NaH ME rats (given the vehicle of formulation B), and the MBZ-NaH ME animals (receiving the MBZ-loaded microemulsion formulation). The treatments were applied by intranasal administration beginning on day 7. **b** Semiquantitative analysis of the relative fluorescence intensity of IRDye 800CW RGD in tumors from the control, NaH ME, and MBZ-NaH ME groups. The data are expressed as the mean ± SEM of three animals. *Significant difference ($p < 0.05$)

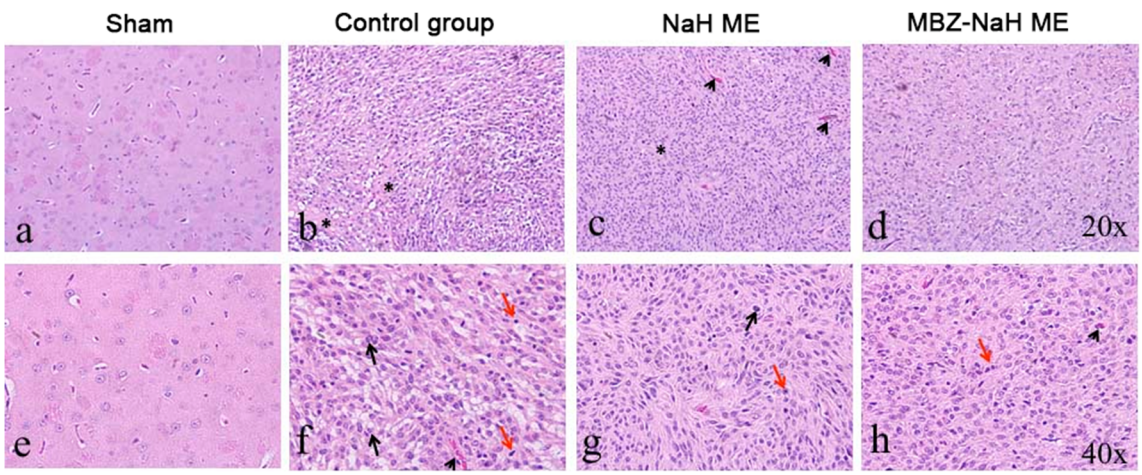

Fig. 10. Hematoxylin and eosin (H&E) staining of glioma tissue after the different treatments: sham (without glioma cells and in the absence of treatment), control (with implantation of glioma cells and in the absence of treatment), NaH ME (the vehicle of formulation B), and MBZ-NaH ME (MBZ-loaded microemulsion formulation). Mitosis (black arrow), necrosis (asterisk), nuclear pleomorphism (red arrow), and vascularity (arrowhead). Magnification × 20 (**a**–**d**) and × 40X (**e**–**h**). (scale bar = 50 μm)

Histological Analysis

Compared to the sham group, the tissues of the control and NaH ME groups exhibited malignant histological features, including alterations in the shape and size of cells (pleomorphism), hypercellularity, mitotic activity, and necrosis. In contrast, cellularity, pleomorphism, and mitosis were low in the rats treated with MBZ-NaH ME (Fig. 10). Since glioblastoma tumors are usually poorly delineated in the presence of an elevated level of vascularity and necrosis, the current results suggest that the application of the MBZ-NaH ME formulation decreases the degree of malignancy. However, specific proliferation and vasculature markers are required to corroborate this tentative conclusion.

CONCLUSION

An MBZ-loaded microemulsion was developed for nasal administration. The MBZ formulation, which included OA and Labrafil M 2125 (1:1) as the oily phase and 0.1% of NaH as a mucoadhesive agent, is appropriate for nasal administration according to its physicochemical characterization. The present data reveal that the MBZ-NaH ME treatment afforded an increased survival time of the animals, the reduction of tumor uptake of IRDye 800CW RGD, and the absence of nasal toxicity. Hence, MBZ intranasal delivery could be a promising alternative in glioblastoma therapy. Future studies are required to understand *in vivo* biodistribution of MBZ and its mechanisms of transport to the brain.

ACKNOWLEDGMENTS

The authors are grateful to Gateffosse (Químicos Lyontec) for the donation of Transcutol HP, Labrafac, Labrafil M 2125, Labrafil and Peceol excipients, and to Croda Inc. (Química Croda) for the donation of super-refined oleic acid and docosahexaenoic acid. We greatly appreciate the support provided by the staff at USAII UNAM to characterize mebendazole.

FUNDING

This study was financially supported by UNAM-DGAPA-PAPIIT: IN223817. Student grant (257882) was provided to Julio Mena by CONACYT during the study.

COMPLIANCE WITH ETHICAL STANDARDS

Conflict of Interest The authors declare that they have no conflict of interest.

REFERENCES

1. Bianco J, Bastiancich C, Jankovski A, des Rieux A, Préat V, Danhier F. On glioblastoma and the search for a cure: where do we stand? Cell Mol Life Sci. 2017;74:2451–66.
2. Stupp R, Mason WP, van den Bent MJ, Weller M, Fisher B, Taphoorn MJ, et al. Radiotherapy plus concomitant and adjuvant temozolomide for glioblastoma. N Engl J Med. 2005;352:987–96.
3. Abbott NJ, Patabendige AA, Dolman DE, Yusof SR, Begley DJ. Structure and function of the blood–brain barrier. Neurobiol Dis. 2010;37:13–25.
4. Guerini AE, Triggiani L, Maddalo M, Bonù ML, Frassine F, Baiguini A, et al. Mebendazole as a candidate for drug repurposing in oncology: an extensive review of current literature. Cancers. 2019;31:1262–84.
5. Bai RY, Staedtke V, Aprhys CM, Gallia GL, Riggins GJ. Antiparasitic mebendazole shows survival benefit in 2 preclinical models of glioblastoma multiforme. Neuro-Oncology. 2011;13:974–82.
6. Dayan AD. Albendazole, mebendazole and praziquantel. Review of non-clinical toxicity and pharmacokinetics. Acta Trop. 2003;86:141–59.
7. Kumar N, Lochhead J, Pizzo M, Nehra G, Boroumand S, Greene G, et al. Delivery of immunoglobulin G antibodies to the rat nervous system following intranasal administration: distribution, dose-response, and mechanisms of delivery. J Control Release. 2018;286:467–84.
8. Khatoon M, Farhan M, Shahnaz G, Rehman F, Din F, Rehman A, et al. Development and evaluation of optimized thiolated chitosan proniosomal gel containing duloxetine for intranasal delivery. AAPS PharmSciTech. 2019;20:276–88.
9. Crowe TP, West MHG, Kanthasamy AG, Hsu WH. Mechanism of intranasal drug delivery directly to the brain. Life Sci. 2018;195:44–52.
10. Bruinsmann FA, Richter Vaz G, Soares Alves AS, Aguirre T, Polhmann AR, Stanisçuaski GS, et al. Nasal drug delivery of anticancer drugs for the treatment of glioblastoma: preclinical and clinical trials. Molecules. 2019;24:4280–312.
11. van Woensel M, Wauthoz N, Rosière R, Amighi K, Mathieu V, Lefranc F. Formulation for intranasal delivery of pharmacological agents to combat brain disease: a new opportunity to tackle GBM? Cancers. 2013;5:1020–48.
12. Sabir F, Ismail R, Csoka I. Nose-to-brain delivery of antiglioblastoma drugs embedded into lipid nanocarrier systems: status quo and outlook. Drug Discov Today. 2020;25:185–94.
13. Callender SP, Mathews JA, Kobernyk K, Wettig SD. Microemulsion utility in pharmaceuticals: implications for multi-drug delivery. Int J Pharm. 2017;526(1–2):425–42.
14. Hosny KM, Hassan AH. Intranasal in situ gel loaded with saquinavir mesylate nanosized microemulsion: preparation, characterization, and in vivo evaluation. Int J Pharm. 2014;475:191–7.
15. Shinde RL, Bharkad GP, Devarajan PV. Intranasal microemulsión for targeted nose to brain delivery in neurocysticercosis: role of docosahexaenoic acid. Eur J Pharm Biopharm. 2015;96:363–79.
16. Gadhavea D, Gorainb B, Tagalpallewara A, Kokarea C. Intranasal teriflunomide microemulsion: an improved chemotherapeutic approach in glioblastoma. J Drug Deliv Sci Technol. 2019;51:276–89.
17. Llaguno MM, Romero PM, Serrano BJ, Medina LA, Uribe UN, Salazar AM. Mifepristone overcomes tumor resistance to temozolomide associated with DNA damage repair and apoptosis in an orthotopic model of glioblastoma. Cancers. 2018;11:1–16.
18. Paxinos G, Watson C. The rat brain in stereotaxic coordinates. 4th ed. New York: Academic Press; 1998.
19. Stenslik MJ, Potts LF, Sonne JW, Cass WA, Turchan-Cholewo J, Pomerleau F, et al. Methodology and effects of repeated intranasal delivery of DNSP-11 in a rat model of Parkinson's disease. J Neurosci Methods. 2015;15:120–9.
20. Himmelreich M, Rawson BJ, Watson TR. Polymorphic forms of mebendazole. Aust J Pharm Sci. 1977;6:123–5.
21. Bai RY, Staedtke V, Wanjiku T, Rudek MA, Joshi A, Gallia GL, et al. Brain penetration and efficacy of different mebendazole polymorphs in a mouse brain tumor model. Clin Cancer Res. 2015;21:3462–70.
22. Chen JM, Wang ZZ, Wu CB, Lia S, Lu TB. Crystal engineering approach to improve the solubility of mebendazole. CrystEngComm. 2012;14:6221–9.
23. Calvo NL, Kaufman TS, Maggio RM. Mebendazole crystal forms in tablet formulations. AnATR-FTIR/chemometrics

approach to polymorph assignment. J Pharm Biomed Anal. 2016;122:157–65.
24. Liebenberg W, Dekker TG, Lötter AP, de Villiers MM. Identification of the mebendazole polymorphic form present in raw materials and tablets available in South Africa. Drug Dev Ind Pharm. 1998;24:485–8.
25. Brits M, Liebenberg W, de Villiers MM. Characterization of polymorph transformations that decrease the stability of tablets containing the WHO essential drug mebendazole. J Pharm Sci. 2010;99:1138–51.
26. de la Torre-Iglesias PM, García-Rodriguez JJ, Torrado G, Torrado S, Torrado-Santiago S, Bolás-Fernández F. Enhanced bioavailability and anthelmintic efficacy of mebendazole in redispersible microparticles with low-substituted hydroxypropylcellulose. Drug Des Devel Ther. 2014;8:1467–79.
27. Pathak R, Dash RP, Misra M, Nivsarkar M. Role of mucoadhesive polymers in enhancing delivery of nimodipine microemulsion to brain via intranasal route. Acta Pharm Sin B. 2014;4:151–60.
28. Nasr M. Development of an optimized hyaluronic acid-based lipidic nanoemulsion co-encapsulating two polyphenols for nose to brain delivery. Drug Deliv. 2016;23:1444–52.
29. Zhang Q, Jiang X, Jiang W, Lu W, Su L, Shi Z. Preparation of nimodipine-loaded microemulsion for intranasal delivery and evaluation on the targeting efficiency to the brain. Int J Pharm. 2004;275:85–96.
30. Sharma G, Mishra AK, Mishra P, Misra A. Intranasal cabergoline: pharmacokinetic and pharmacodynamic studies. AAPS PharmSciTech. 2009;10:1321–30.
31. Mitra R, Pezron I, Chu WA, Mitra AK. Lipid emulsions as vehicles for enhanced nasal delivery of insulin. Int J Pharm. 2000;205:127–34.
32. Chen YS, Chiu YH, Li YS, Lin EY, Hsieh DK, Lee CH, et al. Integration of PEG 400 into a self-nanoemulsifying drug delivery system improves drug loading capacity and nasal mucosa permeability and prolongs the survival of rats with malignant brain tumors. Int J Nanomedicine. 2019;14:3601–13.
33. Shinde RL, Devarajan PV. Docosahexaenoic acid-mediated, targeted and sustained brain delivery of curcumin microemulsion. Drug Deliv. 2017;24:152–61.
34. Horvát S, Fehér A, Wolburg H, Sipos P, Veszelka S, Tóth A, et al. Sodium hyaluronate as a mucoadhesive component in nasal formulation enhances delivery of molecules to brain tissue. Eur J Pharm Biopharm. 2009;72:252–9.
35. Danaei M, Dehghankhold M, Ataei S, Davarani HF, Javanmard R, Dokhani A, et al. Impact of particle size and polydispersity index on the clinical applications of lipidic nanocarrier systems. Pharmaceutics. 2018;10:40–57.
36. Costantino HR, Illum L, Brandt G, Johnson PH, Quay SC. Intranasal delivery: physicochemical and therapeutic aspects. Int J Pharm. 2007;337:1–24.
37. Furubayashi T, Inoue D, Kamaguchi A, Higashi Y, Sakane T. Influence of formulation viscosity on drug absorption following nasal application in rats. Drug Metab Pharmacokinet. 2007;22:206–11.
38. Le TNT, Lim H, Hamilton AM, Parkins KM, Chen Y, Scholl TJ, et al. Characterization of an orthotopic rat model of glioblastoma using multiparametric magnetic resonance imaging and bioluminescence imaging. Tomography. 2018;4:55–65.
39. Grobben B, De Deyn PP, Slegers H. Rat C6 glioma as experimental model system for the study of glioblastoma growth and invasion. Cell Tissue Res. 2002;310:257–70.
40. Gieryng A, Pszczolkowska D, Bocian K, Dabrowski M, Rajan WD, Kloss M, et al. Immune microenvironment of experimental rat C6 gliomas resembles human glioblastomas. Sci Rep. 2017;7:17556–70.
41. Natali F, Siculella L, Salvati S, Gnoni GV. Oleic acid is a potent inhibitor of fatty acid and cholesterol synthesis in C6 glioma cells. J Lipid Res. 2007;48:1966–75.
42. Bryceson AD, Woestenborghs R, Michiels M, van den Bossche H. Bioavailability and tolerability of mebendazole in patients with inoperable hydatid disease. Trans R Soc Trop Med Hyg. 1982;76:563–4.
43. Chen X, Conti PS, Moats RA. In vivo near-infrared fluorescence imaging in integrin αvβ3 in brain tumor xenografts. Cancer Res. 2004;64:8009–14.
44. Huang R, Vider J, Kovar JL, Olive DM, Mellinghoff IK, Mayer-Kuckuk P. Integrin αvβ3-targeted IRDye 800CW near-infrared imaging of glioblastoma. Clin Cancer Res. 2012;18:5731–40.